16th International Flow Measurement Conference, FLOMEKO 2013

24-26th September 2013, Paris

NUMERICAL AND EXPERIMENTAL INVESTIGATION OF FLOW FIELDS IN CRITICAL FLOW SMALL SIZE NOZZLES

E. von Lavante, J. Allofs and F. Winzösch, Univ. of Duisburg-Essen, Germany
R. Kramer and B. Mickan, PTB, Braunschweig, Germany

Abstract

Due to their long term stability, well understood flow behaviour and very low uncertainty, standard critical flow Venturi nozzles (CFVN) are enjoying great popularity as a calibration tool and flow metering device. Their application to very small flow rates beyond the ISO 9300 Standard, however, leaves many questions unanswered. The present work aimed at detailed investigation of flow fields within CFVNs of diameters between 15 µm and 80 µm. The present numerical flow simulations were validated by corresponding experimental work carried out at the PTB.

Keywords: critical flow Venturi nozzles, numerical flow simulation, micro flow rates

Introduction

The use of sonic nozzles in metrology, including the application range and shape of the nozzles, is regulated by the standard ISO 9300 [1]. According to this standard, the validity range of the employment of CFVNs is limited to Reynolds numbers between 10^5 and 10^7. Many times, however, it is desirable to use nozzles at much smaller Reynolds numbers, either for applications with very small volumetric flow rates or for metering gases at very small pressures. In these cases, several investigators [2, 3, 4] have discovered flow effects that were inconsistent with the standard ISO 9300. These included variation of the discharge coefficient C_D as a function of the nozzle back pressure not explainable by the theory offered in ISO 9300, occurrence of instabilities and temporary unchoking of the nozzle. After calibration, however, the same nozzles still offer very reliable means of gas metering. The application range of the CFVNs can be extended beyond the ISO 9300 since the nozzles of the standard shape can be manufactured for throat diameters as low as 80 µm. By lowering the exit pressure well below the values recommended by ISO 9300, they can be still reliably operated, resulting in volumetric flow rates down to Q_V = 100 cm^3/min . For even smaller flow rates down to approximately Q_V = 5 cm^3/min, nozzles of throat diameters as small as d_{throat} = 15 µm must be manufactured using simplified shapes. The present nozzle shapes will be discussed in the next chapter.

These extremely small sonic nozzles (assuming critical conditions at the throat) still possess the same basic advantages of their larger counterparts. They represent a robust, consistent, simple and reliable
means of metering gases and, after proper calibration, are potentially highly accurate. Their practical application to the determination of small flow rates and the generation of gas mixtures on micro scales has been demonstrated by Kramer, Mickan and Schmidt [5]. Here, the very small CFVNs were calibrated using laminar flow elements (LFE) and used singly as well as in series, providing a transfer standard of low uncertainty and high reliability.

The good experience made by the present authors as well as many other investigators with small sonic nozzles employed in metrology justified further study of the corresponding flow fields. It was hoped to gain more detailed knowledge of the behavior of these nozzles when applied to meter small mass flows. This, in turn, should make an explanation of most of the unusual effects occurring in these configurations possible.

According to classical theory which, at first, assumes quasi-one-dimensional flow in the nozzle, the critical mass flow rate is obtained from:

$$\dot{m}_{ideal} = A_{throat} \cdot a^* \cdot \rho^* = A_{throat} \cdot \frac{p_0}{\sqrt{RT_0}} \cdot \psi_r \qquad (1)$$

where a^* is the critical speed of sound, P_0 and T_0 are the total pressure and temperature, respectively, and Ψ is the critical flow function for real gas. The flow rate in real nozzle is different, however, due to boundary layer

displacement, multi-dimensional effects, unsteady flow field and possibly thermal non-equilibrium. It is, therefore, corrected by a so called discharge coefficient C_D:

$$\dot{m}_{real} = c_D \cdot A_{throat} \cdot \frac{p_0}{\sqrt{RT_0}} \cdot \psi_r \qquad (2)$$

Equation (2) is generally used for the determination of the mass flow rate in CFVNs, the discharge coefficient being of great importance. Most of the investigations of CFVNs aim, therefore, at accurate computation or prediction of the discharge coefficient.

With this motivation in mind, the present authors undertook an experimental and numerical investigation of air flow in sonic micro-nozzles, characterized by extremely small Reynolds numbers given by nozzle diameters in the range of 15 – 80 µm. In addition to the flow simulation program ACHIEVE developed by the first author, the commercial program adapco Star CCM+ has been used. Both programs delivered comparable results. The results obtained by the present numerical flow simulations were validated in several cases by the corresponding experimental work performed at the PTB. The close cooperation between the experimental and numerical parts of this study was of advantage when explaining some of the physical phenomena occurring in these nozzles.

Description of cases studied

In the present work, CFVNs of simplified shapes were investigated by numerical flow simulation and experimental flow rate determination having following throat diameters: 15, 25, 35, 40, 50 and 80 µm. The flow in these nozzles was simulated for two exit pressure ratios: p_2/p_0 = 0.4 and 0.3; the experimental work was carried out for a pressure ratio range between 0.07 and 0.95. The nozzles were operated in their forward flow direction (F), in Fig. 1 from left to right, and their backward direction (B), in Fig. 1 from right to left.

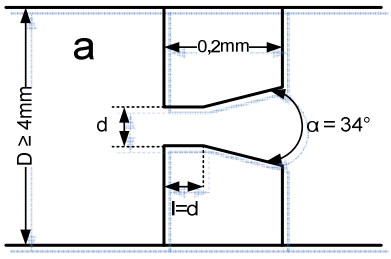

Fig. 1:Geometry of the present nozzles

A REM photograph of one of the punched nozzles with the diameter of approximately 30 µm can be seen in Fig. 2.

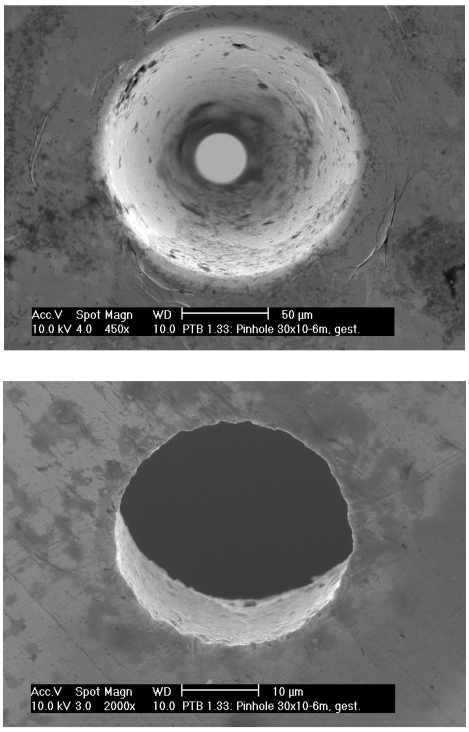

Fig. 2: REM photographs of 30 µm nozzle

In most cases the gas being metered was dry air at atmospheric conditions at the inflow, representing also total pressure and temperature as the pipe supplying the air was much larger than the nozzle diameter. In some experiments, instead of implementing suction (lower outflow pressure) a higher pressure was imposed in the inflow. The Reynolds numbers corresponding to the above cases ranged from Re = 267 (d_{throat} = 15 µm) to Re = 1049 (d_{throat} = 80 µm). Clearly, in all cases the flow was laminar. Having high speed flow in very small configurations, it is important to determine if the flow can still be considered as continuum. The non-dimensional number characterizing the type of flow (continuum – rarefied gas) is the Knudsen number, defined as Kn = λ/L, where λ is the molecular mean free path and L a global reference length, in this case the throat diameter. Alternatively, the Knudsen number can be computed from [6]:

$$Kn = 1,28 \cdot \sqrt{\kappa} \cdot \frac{Ma}{\mathrm{Re}} \qquad (3)$$

Using equation (3), and substituting the present Reynolds numbers, the Knudsen numbers are for the throat conditions:

Kn = 0.006 (d_{throat} = 15 µm)

Kn = 0.0022 (d_{throat} = 80 µm)

The limiting condition for the existence of continuum fluid is Kn < 0.01, indicating that the smallest nozzle was very close to the limit of continuum mechanics.

The very low Reynolds numbers indicated that the flow was laminar with the viscous effects dominating. Consequently, the numerical flow simulations had to be carried out using a method that displayed very low numerical dissipation, yet was still stable for very large flow gradients within the nozzle throat and was capable of accurately capturing the compressible effects in the flow field. Additionally, the method should have been time accurate, as there were possibly high frequency unsteady effects present. These requirements imply that previously, the present investigators had to revert to the code named ACHIEVE, developed by, among others, the first author. The program was fully parallelized using domain decomposition, working with block structured grids. Reasonable computational efficiency was achieved by multi-stage time stepping with optimized Runge-Kutta coefficients. More recently, the coupled (compressible) solver Star CCM+ proved to be capable of delivering comparable results.

The numerical grid generation was accomplished using an elliptic grid generation program developed by the first author and subsequently refined by Allofs [7]. The grids had to offer very high resolution of the high flow gradients at the in- and outflow corners of the throat, resulting in between 20,000 and 40,000 cells in the two-dimensional axially symmetric computations. The quality of grids was essential for obtaining feasible results from the numerical flow simulations. In CCM+, the inherent grid generator was employed.

Experimental setup

The experimental work used for validation of the present numerical simulations was performed at the PTB. By using high resolution digital barometer as a pressure sensor, very sensitive measurement of intake pressure was possible. During the investigations, the flow rate given by the nozzle was measured by a laminar flow element, installed directly in front of the nozzle. The element used in the present work displayed good repeatability and reproducibility. The repeatability was 0.01 ml/min. Downstream of the nozzle, a control valve and a vacuum pump were installed. The control valve was designed for a very wide flow range. It allowed the stabilization of the pressure at the nozzle outflow resulting in fluctuations smaller than 1 mbar. During the investigation, the observed changes of atmospheric pressure were smaller than 0.05 mbar; hence no corrections of the input pressure were necessary. The flow rate determined by the nozzles was measured in both installation directions 5 times, beginning at the lowest output pressure. For the same pressure ratios, no differences in the readouts were observed, meaning that no shift of the LFE occurred.

The presently employed LFE was calibrated using a piston prover shown in Fig. 3. A new type of piston prover using an actively moved piston was developed for particularly low flow rates. The system allowed the calibration transfer standards like MFE or LFE as well as micro nozzles with an uncertainty of U = 0.05% (k = 2).

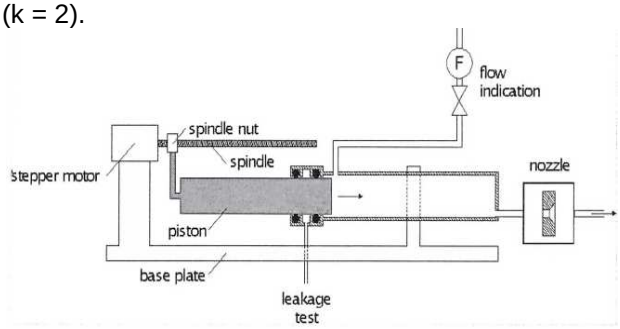

Fig. 3: Schematic picture of the piston prover.

In order to match the flow rate generated by the piston prover to the flow rate determined by a critical nozzle, very stable and sensitive adjustment of the revolution speed of the driving motor was necessary. Adequate properties were achieved by using a stepping motor system. The stepper motor allowed 10 000 steps per rotation. The speed of revolution was changeable by 1 step/rotation.

The flow indication instrument at the intake of the facility was used only for the above mentioned matching of the flow rates. During the calibration, the input valve was closed. If the flow rate of the nozzle and the piston prover were not exactly equal, a slow change of input pressure of the nozzle could be observed. A correction algorithm, taking volume and pressure changes into consideration, allowed achieving the claimed uncertainties even if small pressure changes occurred during the calibration.

Already in the early stage of the experimental work in found that the flow rates in the nozzles

are different depending on the orientation (forward or backward). Accordingly, the experiments were carried out for both orientations of the nozzle.

Experimental results

As of this time, the experiments were completed for following nozzles considered here: 25, 32, 35, 40 and 54 µm. The main problem in evaluating the experimental data is the determination of the hydraulic diameter or, better, the cross-sectional area. As visible in Fig. 2, the nozzle cross-section is irregular, an at the current small size tedious to measure. Only the data of nozzles with positive determination of the effective diameter will be shown here. Below, the flow rates as determined in the experimental work are given in normalized volumetric rate Q_N (at p_0 = 101325 Pa and T_0 = 273.15 K) in ml/min.

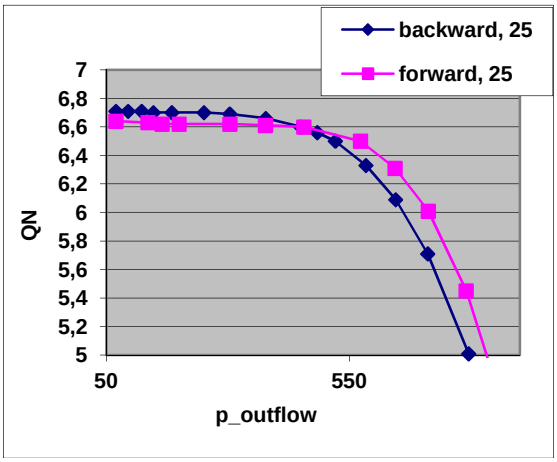

Fig. 4: Flow rate in 32 µm nozzle, ml/min

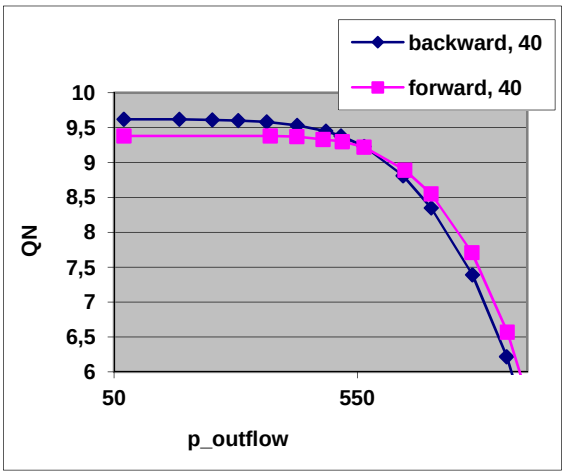

Fig. 5: Flow rate in 40 µm nozzle, ml/min

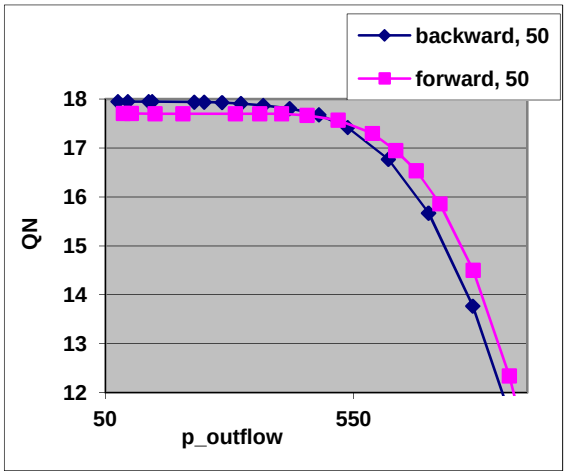

Fig. 6: Flow rate in 54 µm nozzle, ml/min

The outflow pressure is given in mbar; the nozzles in this case were operated in suction mode. In all three cases shown here, there is a difference in behavior between the forward and backward orientation of the nozzles.

Closer inspection of the diagrams reveals that for low pressure ratios p_{out}/p_0 , the nozzles are obviously choked, the mass flow being constant. The mass flow rate in the backward oriented nozzles was consistently higher than in the forward cases (see Fig. 7 for a detailed view of the corresponding part of the diagram). As the outflow pressure is gradually increased, the mass flow rate starts slightly decreasing, indicating that the nozzle starts unchoking.

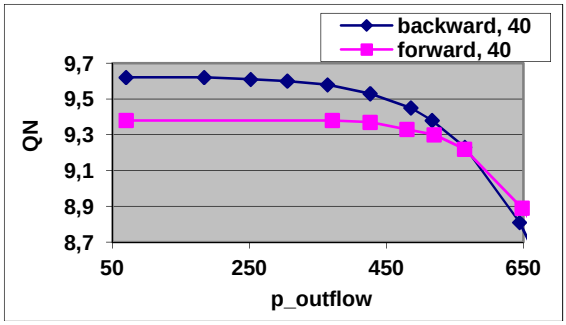

Fig. 7: Detailed view of diagram in Fig. 5

In the backward oriented nozzle case, this occurred earlier than in the forward oriented nozzles. Consequently, there is a "cross-over" point, at which the mass flow rate in the forward case begins to accede the backward case flow rate. In Table 1, the "cross-over" pressure ratio p_{out}/p_0 as well as the corresponding unchoking pressure ratios are given for the three nozzles investigated experimentally.

Clearly, the "cross-over" pressure ratio is a function of the throat diameter or, possibly , the Reynolds number Re_D , but there is still more work required to clarify this issue. As seen in Fig. 4 - 7, the unchoking pressure ratio in backward nozzles is lower than in forward oriented nozzles. In both cases, the the pressure ratio seems to be a weak function of the size of the nozzle, increasing slightly with increasing D_{throat} .

Diameter, µm	Cross-over, mbar	Unch., F, mbar	Unch., B, mbar
32	0.44	0.57	0.45
40	0.511	0.56	0.48
54	0.68	0.59	0.48

Table 1: Significant pressure ratios p_{out}/p_0

Subsequently, the present numerical investigation was carried out in order to explain the above behavior.

Numerical results

The combination of 5 nozzles, backward and forward oriented, with the two exit pressures, resulted in a matrix of 20 cases that were numerically simulated and consequently studied. They are displayed in Table 2. Several interesting facts were observed. All 20 cases considered here were unsteady, with high frequency pressure fluctuations downstream of the throat. The frequency ranged between approximately 300 kHz and 1 MHz, with amplitudes of mass flow fluctuations between 0.03% (basically steady) and 9% (fully unsteady with periodic unchoking). There were at least two different mechanisms behind the unsteady mass flow behavior: in the cases where the throat was always critical, the sonic line was moving stream-wise depending on the changing back pressure, and, on the other hand, in the cases with temporary unchoking of the throat flow, the flow function was changing as a function of time. At the exit pressure ratio of p_{out}/p_0 = 0.3, all the simulated cases were choked at all times; at p_{out}/p_0 = 0.4, all the cases were temporary subcritical in the throat.

In Table 2, the cases presently simulated have been summarized. Obviously, as the throat diameter is increased, the Reynolds number Re_D also increases, with the corresponding decrease of the ratio of boundary layer thickness in the throat δ to the throat diameter D, δ/D. This is a clear indication that the influence of the boundary layer is becoming smaller with increasing size of the nozzle, as expected. Particularly in the case of the smallest nozzle with D = 15 µm, the boundary layer forms more than 35% of the throat radial distance (and, of course, even more of the critical area). The local Knudsen number is in all cases smaller than 0.1, indicating that the concept of continuum can be applied.

diameter [µm]	Reynolds No. Re_d	B.L. thickness δ in [µm]	ratio δ/D	Knudsen number Kn
15	267	5,34	0,35	0,015
25	445	6,90	0,27	0,009
35	623	8,16	0,23	0,007
50	890	9,76	0,195	0,005
80	1049	12,4	0,154	0,003

Table 2: Summary of simulated cases with the corresponding flow parameters

Exemplary for all cases, the flow fields in the 35 µm nozzle will be shown. The first question to be answered is "why is the mass flow rate at choked conditions higher in the backward case" ?

Considering the forward orientation and the pressure ratio p_{out}/p_0 = 0.4 as shown in Fig. 8, and comparing to the same flow conditions in the backward oriented nozzle, it can be concluded that in the forward oriented nozzle, the flow must overcome the sharp corner, generating high vertical velocity component. This results in a thicker boundary layer in the throat, thus reducing the effective mass flow.

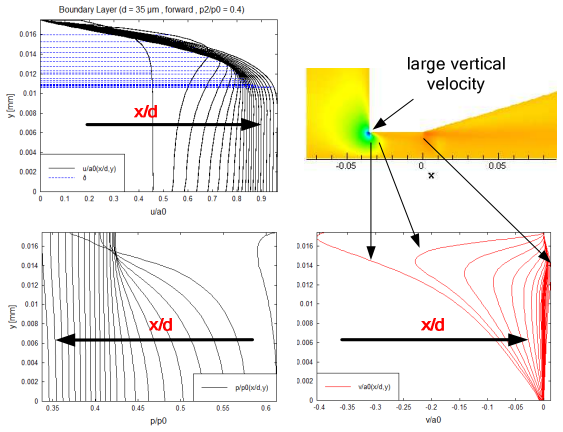

Fig. 8: Horizontal and vertical velocities in the boundary layer in the throat, 35 µm forward oriented nozzle, p_{out}/p_0 = 0.4

The much higher vertical velocity component can be seen in the right, lower picture in Fig. 8 and 9. The thicker boundary layer in the forward orientation can be found consistently in all 20 cases studied numerically.

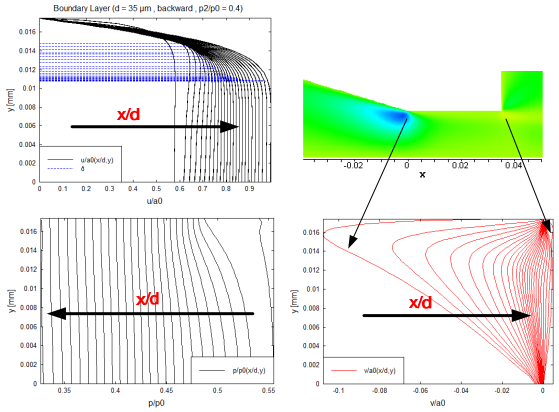

Fig. 9: Horizontal and vertical velocities in the boundary layer in the throat, 35 µm backward oriented nozzle, $p_{out}/p_0 = 0.4$

The second question is "why does the backward oriented nozzle shown signs of unchoking at lower pressure ratios p_{out}/p_0 "? In order to answer this question, one has to consider the flow rate as a function of time in very high resolution, as obtained by the present numerical simulations, shown in Figures 10, 11, 12 and 13.

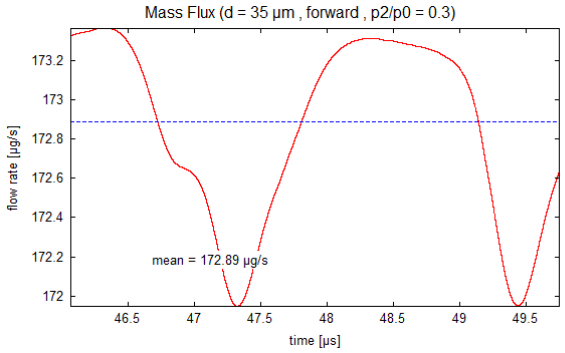

Fig. 10: Mass flow rate in forward oriented nozzle, 35 µm, $p_{out}/p_0 = 0.3$

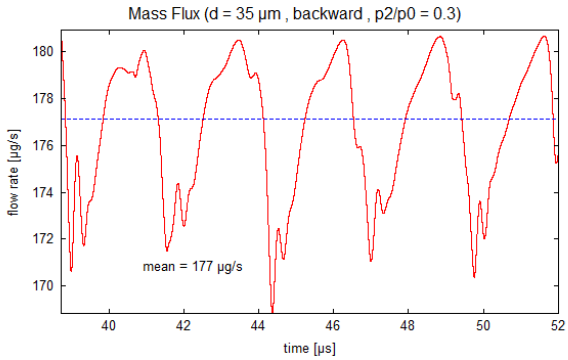

Fig. 11: Mass flow rate in backward oriented nozzle, 35 µm, $p_{out}/p_0 = 0.3$

Although the mass flow rate was always unstable, in the case of the lower pressure ratio, the magnitude of the mass flow fluctuations was very small, being in the case shown 0.2 % and 1.7 %.

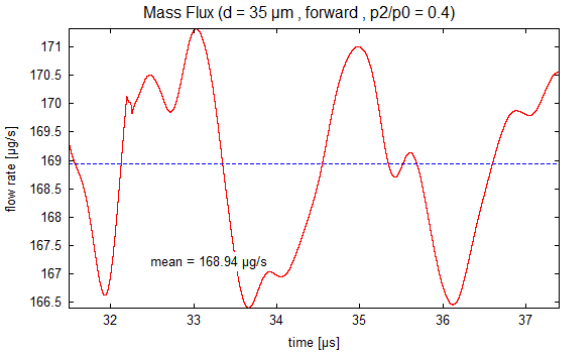

Fig. 12: : Mass flow rate in forward oriented nozzle, 35 µm, $p_{out}/p_0 = 0.4$

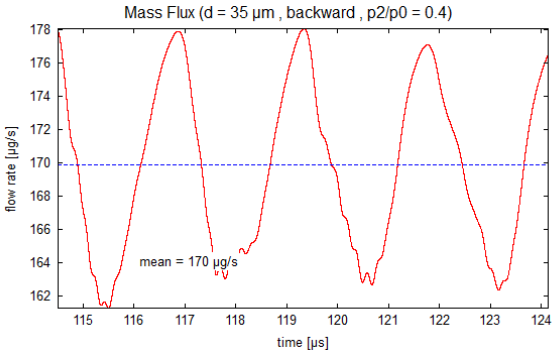

Fig. 13: : Mass flow rate in backward oriented nozzle, 35 µm, $p_{out}/p_0 = 0.4$

In the case of the higher outflow pressure ratio ($p_{out}/p_0 = 0.4$), the magnitude of the mass flow fluctuation was 1.44 % and 4.7 %, respectively. These results lead to two conclusions. Firstly, the backward oriented nozzle, lacking the conical part downstream of the throat, is more susceptible to downstream pressure fluctuations. In the case of the lower pressure ratio p_{out}/p_0 , the flow in the throat remains choked, with the sonic line moving horizontally. As the downstream pressure is increased, the nozzle periodically unchokes, leading to much large fluctuations in the mass flow and, subsequently, to a noticeable drop of the mean value.

The time-wise resolved pictures of the horizontal velocity contours is highly instructive of the above conclusion.

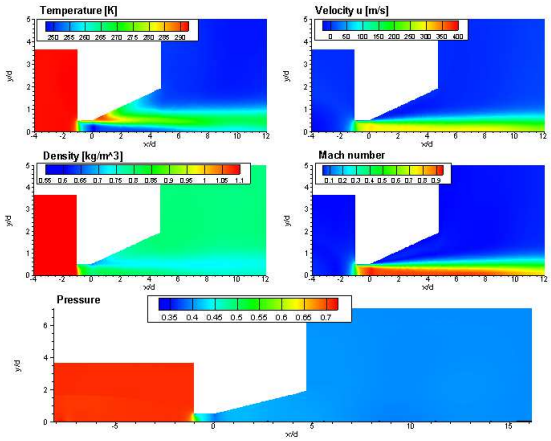

Fig. 14: Flow conditions rate in forward oriented nozzle, 35 µm, $p_{out}/p_0 = 0.4$

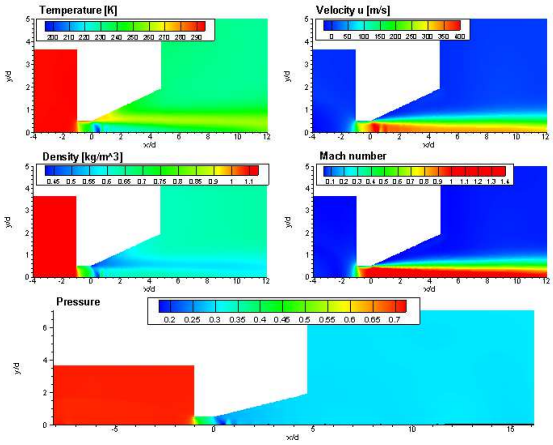

Fig. 15: Flow conditions rate in forward oriented nozzle, 35 µm, $p_{out}/p_0 = 0.3$

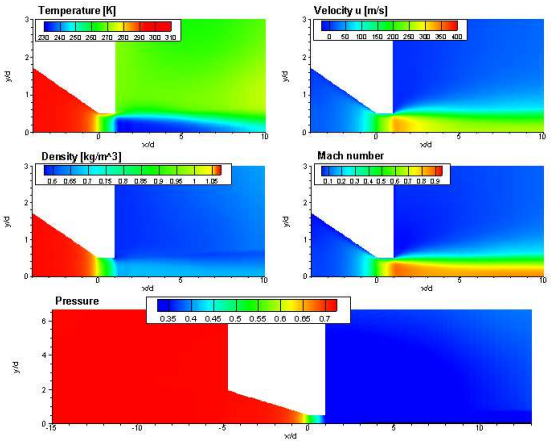

Fig. 14: Flow conditions rate in backward oriented nozzle, 35 µm, $p_{out}/p_0 = 0.4$

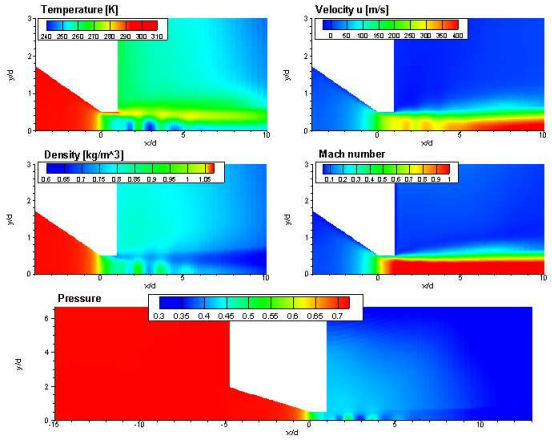

Fig. 14: Flow conditions rate in backward oriented nozzle, 35 µm, $p_{out}/p_0 = 0.3$

The choked condition in the case of $p_{out}/p_0 = 0.3$ can be recognized by considering the Mach disks after the throat, being particularly visible in the backward oriented nozzle.

The behavior of the flow in the nozzles of other throat diameters was similar, making their detailed discussion here superfluous. The most important resulting parameter of the present study was the discharge coefficient C_D. In most experimental studies, including the present one, it was the only reliably measurable parameter in the CFVN. The resulting discharge coefficient C_D as a function of the expression $Re^{-0.5}$ is finally given in Fig. 15 and 16. The relationship displayed in Fig. 15 and 16 should be linear, as the flow is clearly laminar. The numerical results satisfy this requirement, the experimental results show the same tendency of decreasing C_D - coefficient with increasing $1/Re^{0.5}$, but the relationship is non-linear.

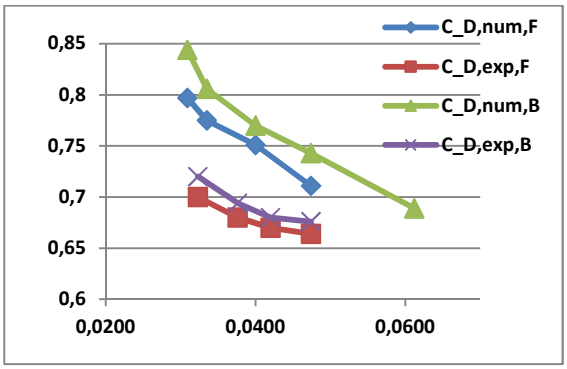

Fig. 15: C_D -coefficient as a function of $(Re)^{-0.5}$, $p_{out}/p_0 = 0.3$

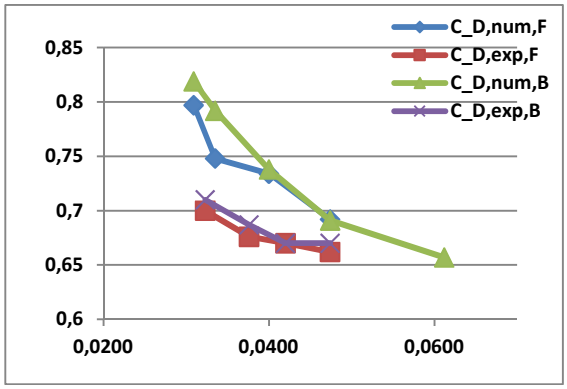

Fig. 15: C_D -coefficient as a function of $(Re)^{-0.5}$, $p_{out}/p_0 = 0.4$

Conclusions

The flow fields in several micro-sized nozzles have been successfully numerically simulated and, in a parallel effort, experimentally investigated. In the experimentally investigated cases, the general agreement between the numerical flow simulations and the experimental data was quantitatively good, showing the correct tendencies. At low pressure ratios (here, $p_{out}/p_0 = 0.3$), the flow in the throat remained critical at all times. At higher pressure ratios, a premature unchoking was observed. The flow was always unsteady, although the fluctuations displayed in some cases very small amplitudes at very high frequencies. For details, the reader is referred to the original publication of Allofs [8]. The execution of the simulations was rather difficult, as the very strong flow variable gradients at the sharp corners of the nozzles required very high computational grid resolution.

The phenomenological questions posed by the experimental work could be answered, leading to logical conclusions about the reasons for the mass flow rate behavior observed in the experiments. At low pressure ratios, the difference in mass flow was due to different thickness of the boundary layer in the throat. At higher pressure ratios, the decreasing flow rate could be explained by time-wise premature unchoking og the nozzles due to pressure fluctuations downstream of the throat.

References

[1] DIN EN ISO 9300:1995, 04.1995: Durchflussmessung von Gasen mit Venturi düsen bei kritischer Strömung.

[2] E. von Lavante, R. Kramer, B. Mickan: “Flow Behavior in Sonic Micro Nozzles”, , Proceedings of Flomeko 2003, Groningen, Netherlands, Mai 2003.

[3] Nakao, Shin-ichi, “Choking Phenomenon of Sonic Venturi Nozzles on Low Reynolds Numbers”, Proceedings of the 9th Int. Conference on Flow Measurement FLOMEKO’98, Lund, 1998.

[4] Wolf, H.; Kramer, R.; Mickan, B. „Mikrodurchfluss – Flussraten im Bereich Mikroliter pro Minute“, Sonderdruck. Braunschweig (119, Heft 1). In: *PTB Mitteilungen, 2009*.

[5] Kramer, R., Mickan, B. and Schmidt, R., „The Application of Critical Nozzles in Series for the Determination of Small Flow Rates and the Generation of Gas Mixtures“, Proceeding of Flomeko 2010, Taipei, Taiwan, 2010.

[6] Hänel, D., „Molekulare Gasdynamik – Einführung in die kinetische Theorie der Gase und Lattice-Boltzmann-Methoden“, Springer Verlag, 2004, page 10.

[7] Allofs, J., „Numerical Simulation of Flow Fields in Critical Flow Micro-Nozzles Used for Flow Metering”, Diplom-Arbeit, Universität Duisburg-Essen, Lehrstuhl für Strömungsmechanik, 2011.

D* [µm]	Q_N,i	C_D,num,F	C_D,exp,F	C_D,num,B	C_D,exp,B
15	1,962			0,689	
25	5,450	0,711	0,664	0,743	0,676
32	8.904		0.670		0.680
35	10,680	0,751		0,770	
40	13,860		0,680		0,694
50	21.78	0,775		0,806	
54	25.40		0.700		0.720
80	55,800	0,797		0,844	

Table 3: Summary of resulting C_D -coefficient, $p_{out}/p_0 = 0.3$

D* [µm]	Q_N,i	C_D,num,F	C_D,exp,F	C_D,num,B	C_D,exp,B
15	1,962			0,657	
25	5,450	0,692	0,662	0,691	0,670
32	8.904		0.670		0.670
35	10,680	0,734		0,738	
40	13,860		0,676		0,687
50	21.78	0,748		0,792	
54	25.40		0.700		0.710
80	55,800	0,797		0,819	

Table 4: Summary of resulting C_D -coefficient, $p_{out}/p_0 = 0.4$